Negative differential resistance behaviour in N-doped crossed graphene nanoribbons*

Chen Ling-Na(陈灵娜)[a)b)], Ma Song-Shan(马松山)[a)], Ouyang Fang-Ping(欧阳方平)[a)], Wu Xiao-Zan(伍小赞)[a)], Xiao Jin(肖 金)[a)], and Xu Hui(徐 慧)[a)†]

[a)] *School of Physics Science and Technology, Central South University, Changsha* 410083, *China*
[b)] *School of Computer Science and Technology, University of South China, Hengyang* 421001, *China*

(Received 22 March 2010; revised manuscript received 6 April 2010)

By using first-principles calculations and nonequilibrium Green's function technique, we study elastic transport properties of crossed graphene nanoribbons. The results show that the electronic transport properties of molecular junctions can be modulated by doped atoms. Negative differential resistance (NDR) behaviour can be observed in a certain bias region, when crossed graphene nanoribbons are doped with nitrogen atoms at the shoulder, but it cannot be observed for pristine crossed graphene nanoribbons at low biases. A mechanism for the negative differential resistance behaviour is suggested.

Keywords: transport properties, negative differential resistance, first-principles, crossed graphene nanoribbons
PACC: 7320A, 7320H, 7335A, 7360T

1. Introduction

Graphene has attracted intensive interest due to its fundamental properties and potential applications in future electronic devices.[1−5] Compared with two-dimensional graphene, graphene nanoribbons (GNRs)[6−10] show distinct electronic properties and can be classified as armchair graphene nanoribbons (AGNRs) and zigzag graphene nanoribbons (ZGNRs). It is found that ZGNRs are metallic for all widths.[11,12] Recently, transport properties of GNRs have received great attention, because they are considered to be one of the most prospective candidates in the nanoelectronic devices. Chemical doping has been revealed to be an influential factor in determining the transport properties of GNRs in nanoscale. Ren *et al.*[13] found the negative differential resistance (NDR)[14−18] behaviour in AGNRs by introducing doping states in the energy gaps of the electrodes. The NDR effect, which features the current decreasing with voltage increasing, has gained applications in a wide range including logic circuits,[19] memory,[20] switching[21] and amplification.[22] Different mechanisms such as chemical changes,[23] local orbital symmetry matching between electrode and scatting region,[24] the channel conduction suppressed at a certain bias,[25] and the bias-induced alignment of molecular orbital[26] have been proposed to explain the NDR behaviour in molecule junctions.

In the present work, we investigate the electronic transport properties for crossed GNRs by applying nonequilibrium Green's functions in combination with the first-principles theory. Here, all edge carbon atoms are saturated with hydrogen atoms and nitrogen atoms are doped at the shoulder or the stem of crossed GNRs. The present work focuses on the doping effect of nitrogen atoms on electronic transport properties for pristine crossed GNRs, N-doped crossed GNRs at the stem, and N-doped crossed GNRs at the shoulder.

2. Method and model

The model structures under study are shown in Fig. 1. Figure 1(a) reveals the pristine crossed GNRs for the M1 system. Figure 1(b) shows the N-doped crossed GNRs at the stem for the M2 system. Figure 1(c) displays the N-doped crossed GNRs at the shoulder for the M3 system and nitrogen atoms are saturated with hydrogen atoms. Figure 1(d) ex-

*Project supported by the National Natural Science Foundation of China (Grant Nos. 10325415 and 50504017), the Natural Science Foundation of Hunan Province, China (Grant No. 07JJ3102), and the Science Develop Foundation of Central South University, China (Grant Nos. 08SDF02 and 09SDF09).
†Corresponding author. E-mail: cmpxhg@mail.csu.edu.cn
© 2010 Chinese Physical Society and IOP Publishing Ltd

hibits the N-doped crossed GNRs at the shoulder for the M4 system These devices are divided into three parts, i.e. left lead, scattering region and right lead. Both leads are semi-infinite GNRs and scattering regions are composed of different N-doped configurations of crossed GNRs. The transport properties of crossed GNRs are investigated based on nonequilibrium Green's function formalism as implemented in ATK (Atomistix Tool Kit),[27] which is based on real-space, nonequilibrium Green's function (NEGF) formalism and the density-functional theory (DFT). The approximation for the exchange–correlation functional is the local density approximation (LDA) with the Perdew–Zunger parametrization. The current can be calculated by the Landauer–Büttiker formula.[28,29] The electrode calculations are performed under periodical boundary conditions, and Brillouin-zone integration is performed by using a $1\times1\times100$ Monkhorst–Pach(MP) grid. Single-ζ basis set is used and a mesh cutoff is set to be 150 Ry to save computational time. Test calculations with larger basis set and cutoff energy are also performed, which give almost the same results.

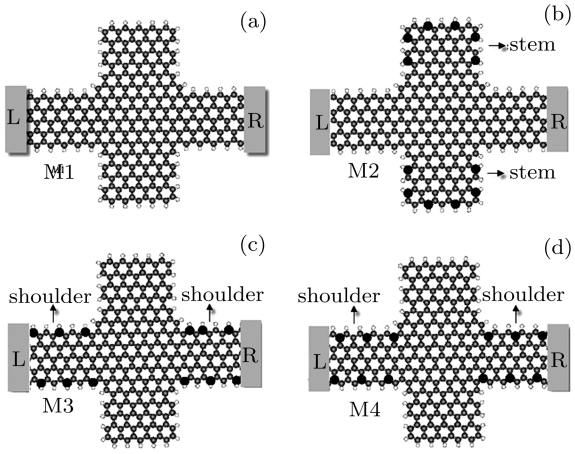


Fig. 1. Schematic diagrams of four crossed GNRs built from a metallic GNRs(shoulder) and semiconducting GNRs (stem), where GNRs are coupled to the left (L) and the right(R) electrodes. (a) pristine crossed GNRs (M1); (b) N-doped crossed GNRs at the stem (M2); (c) N-doped crossed GNRs at the shoulder and nitrogen atoms saturated with hydrogen atoms (M3); (d) N-doped crossed GNRs at the shoulder (M4); The small grey, white, and large black balls correspond to carbon, hydrogen, and nitrogen atoms, respectively.

3. Results and discussion

Figure 2 shows the curves for current as a function of applied bias for all four crossed GNRs. From the figure, we find that M1 and M2 molecular junctions display metallic transport behaviours, while M3 and M4 molecular junctions exhibit semiconductor transport behaviours. We can see clearly that when the bias is lower than $V_{\rm b} = 1.0$ V, the currents are sequenced as follows: M2 > M1 > M4 > M3. In particular, when the bias is lower than $V_{\rm b} = 0.5$ V, the current of M3 is close to zero. This means that at a low bias, N-doped at the stem enhances the electron transport and N-doped at the shoulder significantly suppresses the electron transport. In addition, we find that when the bias $V_{\rm b}$ increases from 0.9 to 1.2 V for M4, the current decreases with the increases of the bias, which shows NDR behaviour in the positive bias range.

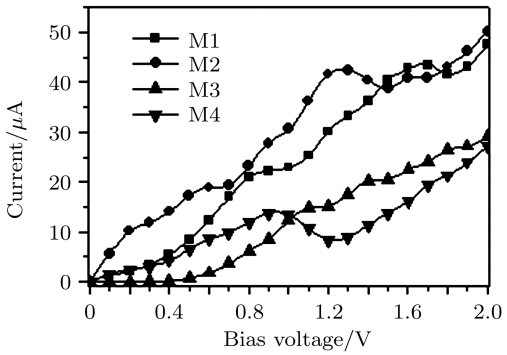


Fig. 2. Curves for current as a function of the positive bias for M1, M2, M3, and M4.

To understand the origin of the transport properties of crossed GNRs, we present the transmission spectra $T(E, V_{\rm b})$ and the projected densities of states (PDOSs) of pristine crossed GNRs and N-doped crossed ZGNRs at zero bias ($V_{\rm b} = 0$) shown in Fig. 3. Figure 3 exhibits very distinct transmission spectra for four different crossed GNRs junctions. It is shown that the transmission peak corresponds to the resonant transmission through the molecular states. The PDOS spectrum provides the information about the lineup of the molecular levels relative to the electrode Fermi energy, and this lineup determines and controls the electron transport across the molecule. From Fig. 3(a), we find that near the Fermi level there are two big transmission peaks which originate from the highest occupied molecular orbital (HOMO) and the lowest unoccupied molecular orbital (LUMO), respectively. Especially, two strong and broad transmission peaks correspond to a strong transmission channel being opened in M1 system. Thus we can infer that there is a strong coupling between electrode and molecule orbital, which dominates the electron transport in M1

system. When more electrons are introduced into the system, it is clearly observed that the frontier molecular orbitals are split into two levels, and more transmission channels are opened. This may lead to more transmission peaks in the system. In fact, it can be found that from Fig. 3(b), more transport peaks appear in the transport spectra for M2 system. However, the M3 junction does not have any transmission peaks near the Fermi energy in Fig. 3(c). We can also see from the PDOS that molecule–electrode interaction does not lead the molecular orbitals for M3 junction to close to the Fermi energy. From Fig. 3(d) we find that one narrow and low transmission peak is located at the Fermi energy for M4. When Fig. 3(d) is compared with Fig. 3(c), with increasing the distance between nitrogen atom and hydrogen atom, the extra non-bonding electron is weakly restricted around N^+. Hence, the impurity state of M4 is closer to the Fermi level than that of M3. It leads the lower transmission to be closer to the Fermi energy for M3 than for M4. The circumstance is quite different from those for M1 and M2 junctions, where both cause HOMO and LUMO to be closer to alignment with the Fermi level. The alignments of the HOMO and the LUMO lead to higher transmissions for M1 and M2.

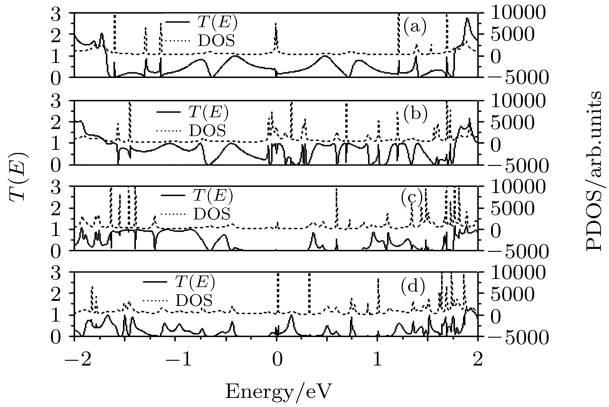


Fig. 3. Transmission coefficients (solid lines) and corresponding PDOSs (dash-dot lines) on the electron energy at zero bias, for M1 (a), M2 (b), M3 (c), and M4 (d).

To understand the NDR behaviour clearly, we present the transmission spectra and the corresponding PDOSs of M4 under biases $V_\mathrm{b} = 0.9$, 1.2, and 1.6 V in Figs. 4(a)–4(c), respectively. The current through a junction is calculated by integrating the transmission coefficient over the bias window: $I = (2e/h)\int_{\mu_{\mathrm{L}(V_\mathrm{b})}}^{\mu_{\mathrm{R}(V_\mathrm{b})}} T(E, V_\mathrm{b})\,\mathrm{d}E$. The transmission coefficient $T(E, V_\mathrm{b})$ is a function of energy level E at a certain bias V_b. The $[\mu_\mathrm{L}(V_\mathrm{b}), \mu_\mathrm{R}(V_\mathrm{b})]$ is the energy region which contributes to the current integration. This is called the bias window or integral window. Consider the fact that Fermi level is set to be zero and the region of the bias window is $[-V_\mathrm{b}/2, +V_\mathrm{b}/2]$. Thus, the current is determined by $T(E, V_\mathrm{b})$ in the bias window, and it is further determined only by the integral area (namely, a shaded area in the bias window). It is clearly seen from Fig. 4 that the each transmission spectrum is composed of a series of peaks, and both the transmission and the PDOS spectra are strongly correlated, especially in the location of their peaks. In Fig. 4(a) we find two broad transmission peaks to enter into the bias window. Compared with the zero-bias case, Fig. 4 shows that for $V_\mathrm{b} = 0.9$ V one transmission peak shifts up 0.4 eV near the Fermi energy and another broad transmission peak at 0.33 eV appears above the Fermi energy. This is the bias corresponding to the current maximum and it indicates the beginning of the NDR. Compared with Fig. 4(a), Fig. 4(b) shows that the total magnitude of transmission coefficient in the bias window becomes smaller, so the NDR behaviour appears in the M4 system. For $V_\mathrm{b} = 1.2$ V, two peaks emerge at 0.06 and 0.18 eV above the Fermi energy, respectively. The transport behaviour is contributed by the low and narrow transmission peaks, which comes from the LUMO and LUMO+1. This bias is that of the current minimum and corresponds to the end of the NDR. From Fig. 4(c), we find new transmission peaks to enter into bias windows, so we can find that the NDR behaviour disappears.

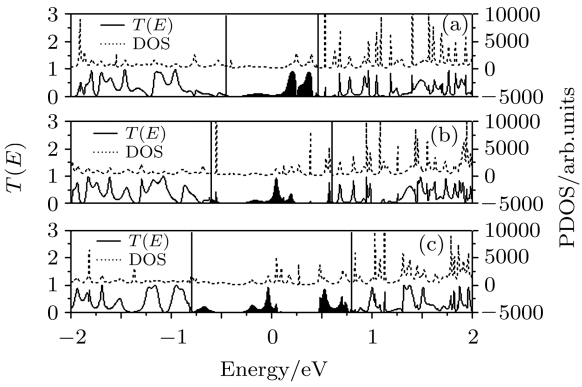


Fig. 4. Transmission coefficients and the corresponding PDOSs for M4 under biases $V_\mathrm{b} = 0.9$ (a), 1.2 (b), and 1.6 V (c). The region between the solid lines is the bias window and the shaded area denotes the integration area in the bias window.

Figure 5 shows a schematic diagram of the alignment of the molecular orbitals that contribute to transmission probabilities of the M4 system relative

to the chemical potentials of the two leads. We note a group of lead states that we refer to as S1 (left) and D1 (right). These states are located within a narrow energy range spanning across the Fermi level. For the junction with zero-bias in Fig. 5(a), the LUMO of scattering region matches the upper edges of two leads, which results in high transmission peaks above the Fermi level. When the bias is increased to 0.9 V in Fig. 5(b), the LUMO catches the tail of right lead and the LUMO+1 catches the edge of right lead. Due to the relatively good matching, the transmission peaks from the LUMO and the LUMO+1 become broader and higher. When the bias is 1.2 V in Fig. 5(c), the LUMO and the LUMO+1 do not overlap effectively with these states of both leads, which leads to low and narrow transmission peaks above the Fermi energy. When the bias is increased to 1.6 V in Fig. 5(d), the LUMO+4 and the LUMO+5 catch the tail of right lead and the HOMO matches weakly with these states of both leads. According to the results above, we can infer that the NDR behaviour originates from the change in coupling degree between the molecular orbitals and electrode.

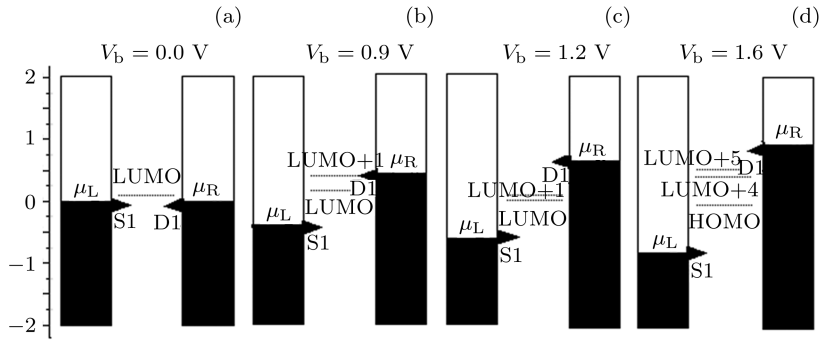


Fig. 5. Schematic diagrams for explaining the mechanism for the NDR. S1 and D1 states and frontier molecular orbits states are denoted in the figures. As the bias increases, the alignments of frontier molecular orbits, S1 and D1 states at four particular positions in biases are shown. The biases of 0.0 (a), 0.9 (b), 1.2 (c) and 1.6 V (d) correspond to equilibrium, current peak, current valley, nonequilibrium in the NDR, respectively.

In order to further understand the NDR behaviour, we present the molecular projected self-consistent Hamiltonian (MPSH). Figures 6(a)–6(c) show three frontier molecular orbits from HOMO to LUMO+1 for the M4 system. From Figs. 6(a) and 6(b), we find that the contributions of LUMO and LUMO+1 to transmission decrease with bias increasing from 0.9 to 1.2 V. Thus there is less current at 1.2 V than at 0.9 V. From Fig. 6(c), we find that the contributions of LUMO and LUMO+1 decrease, but the contribution of HOMO to transmission increases. Additionally, the contributions of additional channels LUMO+4 and LUMO+5 to transmission also increase due to the increase in chemical potential window, which leads to a higher current at 1.6 V than at 1.2 V. According to the above results, we find that the doping inducing a broken symmetry phase of the molecular wave function which leads to a nonlinear change in coupling between molecule and lead is the origin of the NDR.

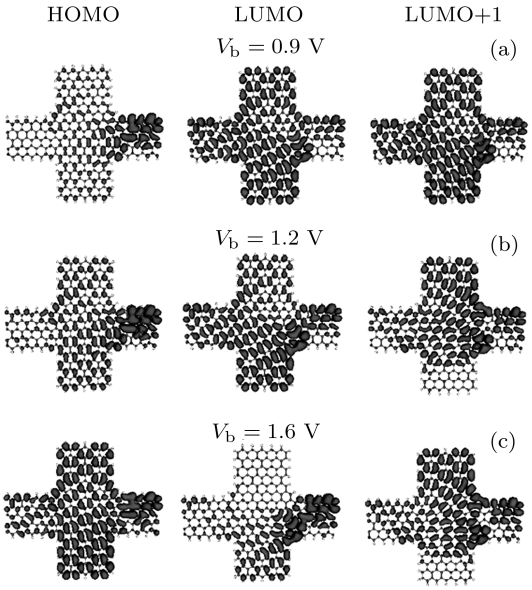


Fig. 6. Frontier orbitals of the MPSH , showing three frontier molecular orbits of the MPSH for M4:. The orbitals are HOMO, LUMO, LUMO+1. The orbitals are under applied bias: 0.9 (a), 1.2 (b), 1.6 V (c). The dark gray corresponds to the negative sign of the wave function.

4. Conclusions

In summary, using the first-principles approach, we find that all the four crossed GNRs display different transport behaviours. At low biases, N-doped crossed GNRs at the stem can enhance the electron transport, while N-doped crossed GNRs at the shoulder can suppress the electron transport. Our calculation in N-doped crossed GNRs reveals the NDR features in the I–V curves. However, the current of pristine crossed GNRs increases with the increase of the bias. These results show that the electronic transport properties of crossed GNRs can be modulated by doped atoms. The electronic transport property depends on doping position. We suggest that doping induces the broken symmetry phase of the molecular wave function, thereby leading to a nonlinear change in coupling between the molecule and lead, which triggers the NDR behaviour.

References

[1] Novoselov K S, Geim A K, Morozov S V, Jiang D, Zhang Y, Dubonos S V, Grigorieva I V and Filrsov A A 2004 *Science* **306** 666

[2] Novoselov K S, Geim A K, Morozov S V, Jiang D, Katsnelson M I, Grigorieva I V, Dubonos S V and Firsov A A 2005 *Nature* **438** 197

[3] Zhang Y B, Tan Y W, Stormer H L and Kim P 2005 *Nature* **438** 201

[4] Berger C, Song Z M, Li X B, Wu X S, Brown N, Naud C, Mayou D, Lit B, Hass J, Marchenkov A N, Conrad E H, First P N and de Heer W A 2006 *Science* **312** 1191

[5] Hu H, Cai J M, Zhang C D, Gao M, Pan Y, Du S X, Sun Q F, Niu Q, Xie X C and Gao H J 2010 *Chin. Phys.* B **19** 037202

[6] Son Y W, Cohen M L and Louie S G 2006 *Nature* **444** 347

[7] Son Y W, Cohen M L and Louie S G 2006 *Phys. Rev. Lett.* **972** 16803

[8] Rosales L, Pacheco M, Barticevic Z, Latgé A and Orellana P A 2009 *Nanotechnology* **20** 095705

[9] Biel B, Blase X, Triozon F and Roche S 2009 *Phys. Rev. Lett.* **102** 096803

[10] Zhou B H, Duan Z G, Zhou B L and Zhou G H 2010 *Chin. Phys.* B **19** 037204

[11] Dutta S, Manna A K and Pati S K 2009 *Phys. Rev. Lett.* **102** 096601

[12] Li Y, cohen M L and Louie S G 2008 *Phys. Rev. Lett.* **101** 186401

[13] Ren H, Li Q X, Luo Y and Yang J L 2009 *Appl. Phys. Lett.* **94** 173110

[14] Pati R, McClain M and Bandyopadhyay A 2008 *Phys. Rev. Lett.* **100** 246801

[15] Zhang X J, Long M Q, Chen K Q, Shuai Z, Wan Q, Zou B S and Zhang Y 2009 *Appl. Phys. Lett.* **94** 073503

[16] Fan Z Q, Chen K Q, Wan Q, Zou B S, Duan W H and Shuai Z 2008 *Appl. Phys. Lett.* **92** 263304

[17] Kim W Y, Kwon S K and Kim K S 2007 *Phys. Rev.* B **76** 033415

[18] Zhang Y, Zhang Y and Zeng Y P 2008 *Chin. Phys.* B **17** 4645

[19] Chen J S, Xu L L, Lin J, Geng Y H, Wang L X and Ma D G 2006 *Semicond. Sci. Technol.* **21** 1121

[20] Su Z S, Fung M K, Lee C S, Li W L and Lee S T 2008 *Appl. Phys. Lett.* **93** 083301

[21] Dimitrakis P, Normand P, Tsoukalas D, Pearson C, Ahn J H, Mabrook M F, Zeze D A, Petty M C, Kamtekar K T, Wang C S, Bryce M R and Green M 2008 *J. Appl. Phys.* **104** 044510

[22] McWhorter A L and Foyt A G 1966 *Appl. Phys. Lett.* **9** 300

[23] Chen J, Reed M A, Rawlett A M and Tour J M 1999 *Science* **286** 1550

[24] Chen L, Hu Z, Zhao A, Wang B, Luo Y, Yang J and Hou J G 2007 *Phys. Rev. Lett.* **99** 146803

[25] Li X F, Chen K Q, Wang L L, Long M Q, Zou B S and Shuai Z 2007 *J. Appl. Phys.* **101** 064514

[26] Cornil J, Karzazi Y and Bredas J L 2002 *J. Am. Chem. Soc.* **124** 3516

[27] Ouyang F P, Xiao J, Guo R, Zhang H and Xu H 2009 *Nanotechnology* **20** 055202

[28] Sahin H and Senger R T 2008 *Phys. Rev.* B **78** 205423

[29] Yan J Y, Zhang P, Sun B, Lu H Z, Wang Z G, Duan S Q and Zhao X G 2009 *Phys. Rev.* B **79** 115403